Available online at www.sciencedirect.com

ScienceDirect

Procedia CIRP 81 (2019) 956–961

www.elsevier.com/locate/procedia

52nd CIRP Conference on Manufacturing Systems

Probabilistic Modelling of Defects in Additive Manufacturing: A Case Study in Powder Bed Fusion Technology

Hossein Mokhtarian[a,b,*], Azarakhsh Hamedi[a], Hari P.N. Nagarajan[a], Suraj Panicker[a], Eric Coatanéa[a], Karl Haapala[c]

[a] Automation Technology and Mechanical Engineering, Tampere University, Finland
[b] University Grenoble Alpes, CNRS, G-SCOP Laboratory, Grenoble, France
[c] School of Mechanical, Industrial, and Manufacturing Engineering, Oregon State University, Corvallis, Oregon, USA

* Corresponding author. Tel.: +358-449711254; E-mail address: hossein.mokhtarian@tuni.fi

Abstract

Implementation of additive manufacturing into product manufacturing suffers from the challenge of part defects prediction. Due to interdependencies of design variables and manufacturing parameters in achieving suitable part quality, modelling methods are necessary to provide simulation capabilities for part quality analysis at early stages of product development. A systematic methodology is proposed to extract cause-effect relationships among variables and to transform this causal model into a Bayesian network. The Bayesian network is then used to predict the effect of specific design and manufacturing parameters on part defects and to estimate the needed input parameters backwards, based on acceptable output values.

Keywords: additive manufacturing; powder bed fusion; probabilistic modeling; bayesian network; dimensional analysis conceptual modeling framework

1. Introduction

Additive manufacturing (AM) processes have transitioned from production of prototypes to functional products, serving various industries, such as automotive, aerospace, machinery, electronics, and medical. Specifically, AM of metal products has seen increased adoption as industrial production systems due to the steady decline in the price of machines and materials [1]. However, AM products have been riddled with defects due to the lack of process knowledge and control systems. In addition, the lack of interoperability in machines has made it difficult to create models that can reduce variations in properties and quality across materials and machine types [2]. Thus, product and process qualification efforts are required to improve product quality and meet industry standards. Part-by-part evaluations are time intensive and new research must focus on creating alternatives to existing conventional qualification methods with the use of validated models and probabilistic methods [3].

AM product quality largely depends on the interactions between design geometry, AM technology, and AM specific process parameters. Metal AM processes, such as laser sintering, function as a multi-parameter dependent process, which require an understanding of the process physics to control variations in final product [4]. In selective laser sintering, a laser beam scans over metal powders, melting and forming layers [4]. However, the lack of high-fidelity models for AM processes results in users choosing parameters based on experimental data collection and expertise. Hence, a non-homogenous temperature gradient is often created, which can lead to spheroidization of the liquid melt pool and residual stress formation, causing cracking, warping, and curling defects in the part [5]. These geometric defects are unavoidable without the use of proper process tuning and control strategies.

10.1016/j.procir.2019.03.234

To help prevent such defects, in-situ monitoring and control systems have been proposed in literature [6], [7]. An increase in the number of control variables is required due to the multi-parameter-dependent nature of powder bed AM.

Toward this end, efforts must be focused on early design stage modeling techniques that can evaluate the interactions between geometry and process parameters early in the design process and aid in informed decision making during process parameter tuning. Such models can help fix high-latency variables in the system at values that minimize their impact on product quality, eliminating the need to control them. Towards that goal, a probabilistic modeling method using Bayesian networks is proposed to model defects in AM parts during laser sintering. The developed model characterizes the effect of geometric and manufacturing parameters on part geometry defects. This model will help designers and manufacturers evaluate the probability of occurrence and the magnitude of defects during manufacturing and support effective tuning of parameters to reduce or eliminate such defects. The method is demonstrated for a case study to model the curling defect in an L-shaped block made of titanium alloy, Ti-6Al-4V, using laser sintering.

The remainder of the manuscript is organized as follows. Section 2 provides a background on defect modeling in laser sintering. Section 3 describes the methodology for the additive manufacturing case study. Section 4 discusses the results of the simulation using the developed Bayesian network for the case study. Section 5 presents the conclusions.

2. Background

Defect modeling for laser powder-bed AM processes is necessary to enable simulations, improve product quality, and eliminate or reduce reject/waste. In laser AM, the temperature-rich environment can result in thermal residual stress formation, leading to geometric errors such as distortion, warping, curing, and spalling. These geometric errors can cause unfinished products and premature failure of product [8].

Research in AM defect modeling has investigated several ways to reduce thermally-induced residual stress and its associated geometric tolerance losses. Vasinota et al. [9] performed thermomechanical modeling and simulation of the laser engineered net shaping process with the help of process maps. They found that uniform preheating of the base plate could reduce residual stresses and achieve optimum melt pool length. Similar research have verified that preheating of the base plate is one of most effective means to reducing residual stresses in AM [10], [11]. In addition to preheating, research has focused on optimizing scan patterns and weld deposition paths to reduce residual stress and deflection. Pohl et al. [5] investigated the effect of processing conditions and material on thermal stresses and part deflection during laser sintering. They found that density or strength of laser-sintered products might contradict the goal of reduced thermal stresses. They also found that different scanning patterns, especially direction of line scan and short raster pattern could reduce deflections in the product.

Nickel et al. [12] investigated the effect of deposition patterns on deflection of the part using finite element modeling. Their study showed that deposition patterns had a significant effect on dimensional quality of the part. They found raster patterns with lines perpendicular to the laser beam's long axis yielded low deflections in the part. More recent research has focused on building support structures to prevent residual stress-induced curling and distortion. Calignano [13] investigated the use of supports for overhang features in selective laser sintering. He posited that additional support is required for overhang features to reduce geometric distortions. However, he suggested that it is necessary to use minimal support structure to obtain the best trade-off between time, cost, and accuracy of production.

Cheng and Chou [14] also investigated overhang support patterns to reduce deformation of overhang parts. They developed a thermomechanical model to simulate deformation in overhang structures in electron beam melting. They found that solid support columns could reduce overhang defect. They also reinforced the notion that a trade-off must be met between reducing deformations and reducing the amount of support materials used to maintain low production costs. In the research presented herein, the use of supports and the effect of support geometry on part deformation is evaluated using a Bayesian network model.

3. Case Study and Methodology

Curling is a recurring defect in laser-based metal AM. It predominantly occurs on overhang surfaces that are not supported by enough material from previous layers. Excessive heat energy input (overheating) leads to a cumulative thermal constraint on the part being processed, resulting in an upward deflection of overhanging features. Suppressing the curling defect entails exploring the design space among parameters related to part geometry, part orientation, support structure, and manufacturing process parameters.

The case study presented here aims at developing a probabilistic model to explore the design space of an L-shaped geometry and to characterize the effect of design parameters on the curling defect during early design stage. The case study follows the workflow shown in Fig. 1. The generic workflow includes three main stages: 1) using the dimensional analysis conceptual modeling (DACM) framework to generate a causal graph of the phenomenon and the associated governing equations, 2) translating the causal graph into directed acyclic graphs (DAGs) for Bayesian network model development, and 3) probabilistic modeling of the curling defect in BayesiaLab software. These stages proceed through five steps, as discussed below.

Step 1: The aim of DACM modeling stage is to extract causal rules and establish governing equations among the variables in the problem using the DACM framework [15], [16]. The problem is evaluated from a functional perspective; a systematic approach to extract causal rules and establish governing equations from a functional model is followed. Fig. 2 shows a functional model where the design space is divided into three domains: cyclic functions of the AM process, useful functions of the support structure, and non-desired functions. The support structure comprises two main functions: the function 'to dissipate' heat energy, similar to a heat sink, and

the function ‘to increase inertia’. Heat energy dissipation is defined here by cooling rate (CR), which depends on the geometry of the support and heat transfer variables. Inertia depends on the geometry of the supports and material density. The non-desired functions of the supports characterize the generation of a thermal constraint that results in the bending moment and the function ‘to resist’ the deflection.

Step 2: Once the functional model is established and variables characterizing those functions are assigned, the algorithms developed in DACM lead to systematic extraction of the cause-effect relationships between the variables and to establishing behavioral laws using dimensional analysis (DA) principles. Fig. 3 represents the extracted causal rules between the variables (nodes) in the form of a causal graph, where independent design variables are shown in green, exogenous variables are shown in gray, and performance variables are shown in red. DA uses cause-effect relationships in the form of (1, as well as dimensions of variables to provide the mathematical relationship among variables in the form of (2, where $\{x_{i1}, x_{i2}, \dots, x_{in}\}$ are the influencing (cause) variables, y_i is the performance (effect) variable, and $\{\alpha_{ij} \mid 1 \le j \le n\}$ are the exponents of the variables. DA seeks for finding suitable exponents for the variables to respect the dimensional homogeneity principle [17].

$$y_i = f\left(x_{i1}, x_{i2}, \dots, x_{ij}\right) \quad 1 \le j \le n \tag{1}$$

$$\pi_{y_i} = y_i . x_{i1}^{\alpha_{i1}} . x_{i2}^{\alpha_{i2}} \dots . x_{ij}^{\alpha_{ij}} \tag{2}$$

The DACM framework also enables integration of existing equations directly to the functional model and causal graph. (3 approximates the temperature difference between layers as a function of heating rate (HR), cooling rate (CR), part geometry variables (W, L, and b), and process parameters (d_l, l_t, v, and t_w).

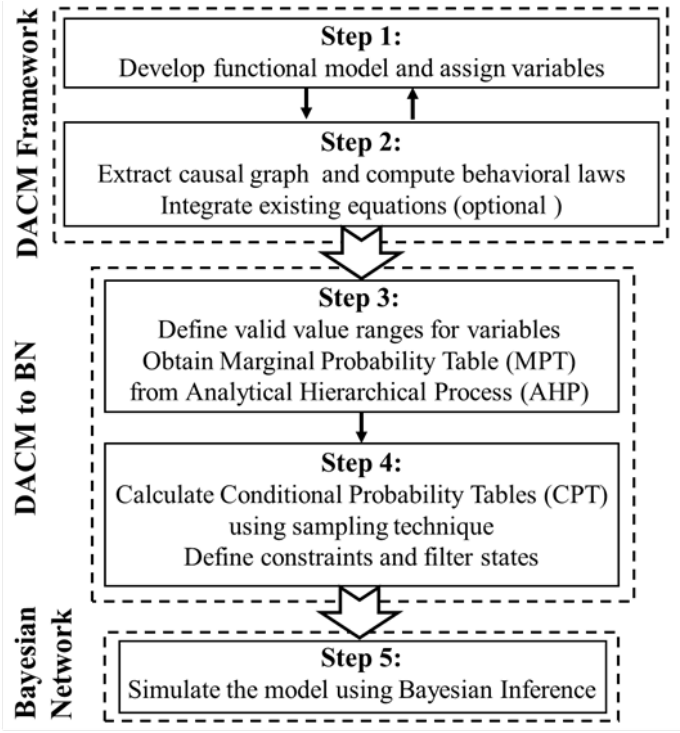

Fig. 1. Methodology workflow.

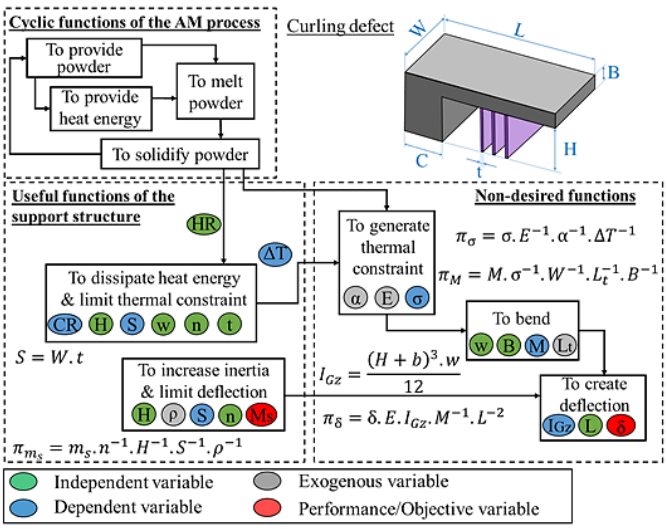

Fig. 2. Functional model for curling defect using DACM Framework.

The equations associated with the functional model shown in Fig. 2 are listed in (3 through (7.

$$\Delta T = \left(\frac{L.W.b}{d_l . l_t . v}\right)\left(HR - CR\right) - \left(\frac{b.t_w}{l_t}\right)\left(CR\right) \tag{3}$$

$$\pi_\sigma = \sigma . E^{-1} . \alpha^{-1} . \Delta T^{-1} \tag{4}$$

$$\pi_M = M . \sigma^{-1} . w^{-1} . L_t^{-1} . b^{-1} \tag{5}$$

$$\pi_\delta = \delta . E . I_{Gz} . M^{-1} . L^{-2} \tag{6}$$

$$\pi_{m_s} = m_s . n^{-1} . H^{-1} . S^{-1} . \rho^{-1} \tag{7}$$

Step 3: This step defines the valid value ranges for the independent variables of the functional model. These ranges are then divided into several intervals, or states. For providing marginal probability tables (MPT) to each interval of the independent variables, it is possible either to assign a random probability of occurrence to each variable interval or to integrate expert knowledge and preferences [18].

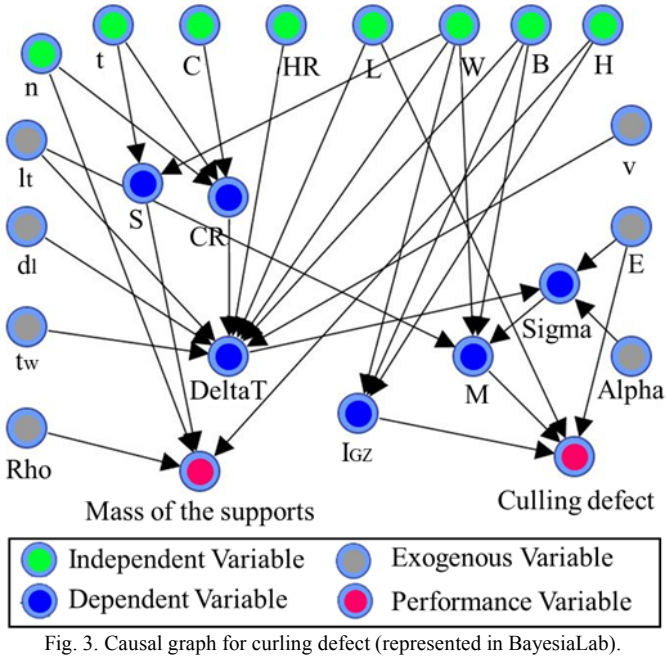

Fig. 3. Causal graph for curling defect (represented in BayesiaLab).

In this study, the analytical hierarchy process (AHP) is used to capture experts' knowledge and preferences in the Bayesian network model [19]. AHP is an efficient tool to deal with complex decision-making problems involving multiple experts and comparisons, since it reduces the complexity of a decision to a series of pairwise comparisons. In this study, experts answered a series of questions by filling AHP tables associated to the required comparisons. The aim was to capture the experts' preferences over different intervals for each independent variable. To enhance this process, AHP tables were transformed into a series of questions. For instance, supposing four intervals (i=4) were defined for the number of supports (n), the questions would be formulated to capture expert preferences over the intervals two-by-two (e.g., interval 1 vs. interval 2), as follows: 'Considering all conditions for printing a desired part, what is your preference of interval 1 compared to interval 2?' The questions were repeated ((i^2-i)/2) times to obtain two-by-two comparisons of all intervals for all independent variables.

Once all preferences were captured from pairwise comparisons, AHP was used to generate a weight for each interval, in a way that the sum of all individual interval weights is equal to one. Hence, the weights generated by AHP are equivalent to the probability of selection of that interval by experts. The process of capturing experts' preferences continues to cover all independent variables. Table 1 provides the list of variables of the case study with their associated units, ranges of values, marginal probabilities, and equations.

Step 4: The causal graph extracted by DACM is a directed acyclic graph (DAG) as an initial Bayesian network prerequisite. However, a few systematic modifications need to be carried out to adapt the DACM causal graph to the Bayesian network model.

First, exogenous variables have a fixed value and do not vary in the system. Therefore, they should be removed from the causal graph. The effect of exogenous variables is not eliminated from the model, since they are considered in the equations as constants. The second modification involves defining the constraints and filter state among variables, which is necessary to avoid impossible combinations of values for independent variables and also to limit the design space. Constraints are defined between parent nodes, and filter states are used as an interval/state within child nodes. The geometric parameters in the case study have been limited using constraints in terms of ratio to avoid the simulation of undesirable geometries. Table 2 represents the acceptable ranges for the design parameters for this case study.

Once the MPTs are established for the independent variables, conditional probability tables (CPTs) are then populated using a sampling technique. The sampling technique starts with calculating the range for the child nodes based on the maximum and minimum value of the parents and the governing equations. The range of values for CPT is then divided into several intervals. The sampling technique continues by taking a number of samples from the parent nodes. The process uses the governing equations for each interval in parent node(s) to calculate the corresponding value in the child node(s). Finally, filtering the impossible values for each child node is essential to avoid propagation of error in the network.

Table 1. List of case study variables with range of values and equations.

Variable (Symbol)	Unit	(Range of values)/Equations **Marginal Probability (%)**		
Part length (L)	mm	(15, 45) **11.11**	(45, 75) **66.67**	(75, 120) **22.22**
Part height (H)	mm	(3, 9) **9.53**	(9, 18) **24.99**	(18, 36) **65.48**
Part width (W)	mm	(3, 9) **23.85**	(9, 18) **62.50**	(18, 36) **13.65**
Part base (C)	mm	(4, 12) **10.95**	(12, 21) **30.90**	(21, 33) **58.16**
Part thickness (b)	mm	(2, 6) **19.63**	(6, 12) **65.71**	(12, 18) **14.66**
Support thickness (t)	mm	(0.3, 1) **65.86**	(1, 1.8) **26.28**	(1.8, 3) **7.86**
Number of supports (n)	---	(1, 5)	(6, 10)	(11, 15) (16, 20)
Cooling rate (CR)	°C/s	(18, 25)		
Heating rate (HR)	°C/s	35		
Elasticity modulus (E)	MPa	$113.8 * 10^3$ [20]		
Thermal expansion (α)	1/K	$8.6 * 10^{-6}$ [20]		
Density (ρ)	g/mm^3	$4.43 * 10^{-3}$ [20]		
Powder layer thickness (l_t)	mm	0.1		
Laser diameter	mm	0.115		
Laser scan velocity (v)	mm/s	1000 [14]		
Temperature difference (ΔT)	K	Calculated by Eq. 3		
Thermal constraint (σ)	MPa	Calculated by Eq. 4		
Thermal constraint moment (M)	N.mm	Calculated by Eq. 5		
Curling defect (δ)	mm	Calculated by Eq. 6		
Total support mass (m_s)	g	Calculated by Eq. 7		

Step 5: Bayesian inference for the case study is implemented in BayesiaLab software. The software uses a sampling technique to calculate all possibilities for the variables in the network. The Bayesian inference mechanism enables simulations to observe the effect of user preferences or evidence across a developed network. The simulation of the developed network is presented in Section 4.

Table 2. Initial and defined acceptable value ranges for geometric constraint ratios to limit the design space.

Constraint Ratio	Initial Range	Acceptable Range
C_1=b/L	(0.016, 1.2)	(0.1, 0.2)
C_2=W/L	(0.025, 2.4)	(0.16, 0.5)
C_3=C/L	(0.033, 2.2)	(0.25, 0.5)
C_4=H/L	(0.025, 2.4)	(0.2, 1)
C_5=n.t/L	(0.0025, 4.0)	(0.0025, 0.5)

4. Results and Discussion

With the aid of the Bayesian inference mechanism, the designer can use the developed model in two directions: (1) for predicting the effect of specific design and manufacturing parameters on defects (forward simulation) and (2) for diagnosing the independent variables' most probable value for particular results in performance (backward simulation). Designers are able to visualize the cascading impacts of choices for design variables in real time. This enables the designer to utilize expert knowledge embedded in the model and make a better-informed decision early in the design process.

4.1. Forward simulation

Fig. 4 shows the effect of the design variables on the resulting curling defect for manufacturing of the L-shaped part. During simulation, the values for part height (H, 9-18 mm), width (W, 9–18 mm), length (L, 45-75 mm), and thickness (b, 12-18 mm) are set as evidence for the Bayesian network model.

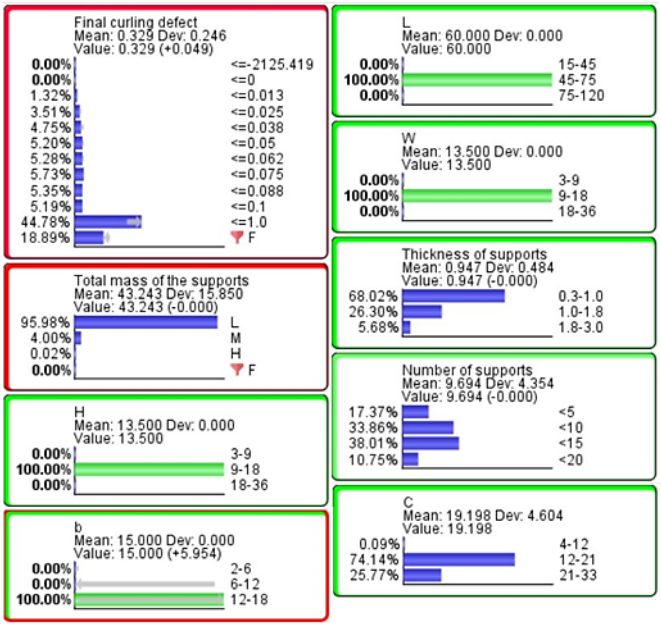

Fig. 4. Predicted effect of part geometric dimensional features on the probability of curling defects for medium-sized parts (45 < L < 75).

For these part dimensions, it is seen that the probability of curling increases in the high value state of the variable (curling <=1.0) to 44.78%. In order to reduce the value of curling defect, the influence of two design variables, part height and part width are investigated. The individual effects of width and height on the curling defect are shown in Figure 5. It is seen that increasing part width is predicted to result in an increased curling defect. Lower range values for part height (3-18 mm) are predicted to increase the magnitude of curling, while high range values (18–36 mm) would reduce the curling defect, due to its non-linear relationship with part curling defect. The non-linearity arises due to the design constraints imposed during modelling. The values for curling defect in Figure 5 are calculated using Eqs. 3-7. The knowledge from Figure 5 can be used to set evidence to the Bayesian Network model and/or inversely to validate the results of the Bayesian inference.

The results obtained from Figure 5 are compared with the result of the Bayesian Network. In Fig. 6, new evidence for part width (W, 18–36 mm) and part height (H, 18-36 mm) are presented to characterize the effect of these changes on the curling defect.

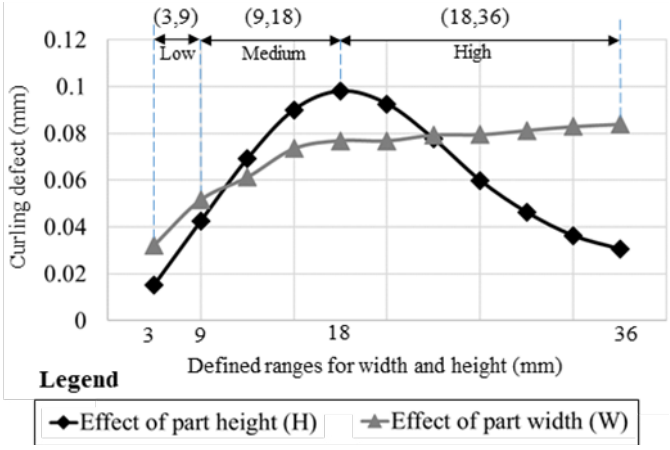

Fig. 5. Effect of part height and part width on the curling defect.

Fig. 6. Predicted effect of part width and part height on the probability of curling defects for medium-sized parts (45 < L < 75) compared to Figure 4.

It is seen that the changes reduced value for curling defect. The probability that the curling defect lies in low value states of the variable (<=0.025, <=0.038, and <=0.05) increased to 22.97%, 21.68%, and 14%, respectively, representing significant decrease in the value of curling defect from the range (0.1 mm - 1 mm) to range (0.013 mm to 0.038 mm). It is to be noted that the Bayesian Network results also highlight the relative importance of design variables on the curling defect. The increase in width increases the curling defect as seen in Figure 5 however, the influence of height on curling defect overshadows the influence of width as seen in Figure 6.

4.2. Backward simulation

During backward simulation, the curling defect was set to be in a low state (<=0.013) and the total mass of supports was set in the low range (<=80 g) for small parts (15< L<45). The effect of this evidence is shown in Fig. 7, where the most probable states for the part and support dimensions are found for the set evidences for length of part, curling defect, and the total mass of supports. For low curling defect and low total mass of supports, the model predicts that part height must be in the high value state (0.3-1.0 mm, with a probability of 72.47%), part thickness in the low value state (2-6 mm, with a probability of 71.31%), part width in medium value state (9-18 mm, with a probability of 74.21%), and the number of supports must be less than or equal to five (with a probability of 57.78%).

5. Conclusion

Bayesian network based defect modelling is beneficial for characterizing complex systems such as the design and production of metal parts through additive manufacturing. The foregoing research develops and demonstrates an approach to generate and explore a Bayesian network model characterizing the influence of design and manufacturing parameters on the

curling defect in laser-based additive manufacturing for an L-shaped part.

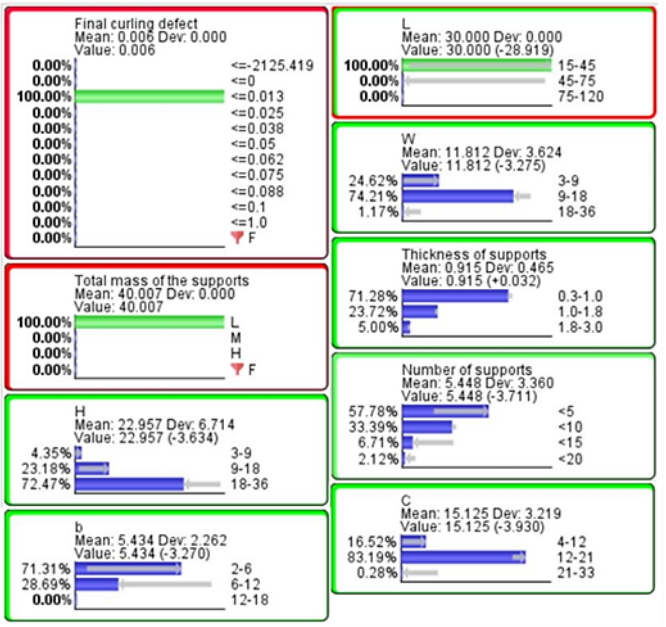

Fig. 7. Backward simulation to minimize curling defect and supports' mass for small-sized parts (15< L <45).

The methodology developed herein is generic and could be expanded to include other geometric defects resulting from non-homogenous temperature gradient in laser additive manufacturing. The Bayesian network allows for two-way monitoring of the modelled system. First, the model estimates the values for targets based on fixed design parameters. Second, it allows the user to set evidence for known targets and then uses the model to backtrack and identify the most probable value ranges for the part geometric dimensions to attain those targets. The simulation of the model helps designers make conscious decisions about changes in product geometry early in the design stage. Such evaluations will eliminate steep costs associated with making design changes late in the production process.

In addition, the results of this study must be used as prior knowledge to calibrate the model with experimental data. For instance, the curling defect is a recursive phenomenon, thus the equations used to model the curling defect uses recursive computation. The model in this research uses approximation to avoid loops in the Bayesian network. Hence, to improve accuracy of the model, future work will focus on training the Bayesian network using data generated through constraint programming for the same governing equations.

References

[1] D. S. Thomas and S. W. Gilbert, "Costs and Cost Effectiveness of Additive Manufacturing," *Spec. Publ. NIST SP - 1176*, Dec. 2014.
[2] W. E. Frazier, "Metal Additive Manufacturing: A Review," *J. Mater. Eng. Perform.*, vol. 23, no. 6, pp. 1917–1928, Apr. 2014.
[3] W. E. Frazier, "Direct digital manufacturing of metallic components: vision and roadmap," presented at the 21st Annual International Solid Freeform Fabrication Symposium, Austin, TX, Aug, 2010, pp. 9–11.
[4] D. D. Gu, W. Meiners, K. Wissenbach, and R. Poprawe, "Laser additive manufacturing of metallic components: materials, processes and mechanisms," *Int. Mater. Rev.*, vol. 57, no. 3, pp. 133–164, May 2012.
[5] H. Pohl, A. Simchi, M. Issa, and H. C. Dias, "Thermal stresses in direct metal laser sintering," in *Proceedings of the 12th Solid Freeform Fabrication Symposium, Austin, TX*, 2001.
[6] P. K. Rao, J. P. Liu, D. Roberson, Z. J. Kong, and C. Williams, "Online real-time quality monitoring in additive manufacturing processes using heterogeneous sensors," *J. Manuf. Sci. Eng.*, vol. 137, no. 6, p. 061007, 2015.
[7] L. Song and J. Mazumder, "Feedback control of melt pool temperature during laser cladding process," *Control Syst. Technol. IEEE Trans. On*, vol. 19, no. 6, pp. 1349–1356, Nov. 2011.
[8] C. Teng *et al.*, "A review of defect modeling in laser material processing," *Addit. Manuf.*, vol. 14, pp. 137–147, 2017.
[9] A. Vasinonta, J. L. Beuth, and M. L. Griffith, "A Process Map for Consistent Build Conditions in the Solid Freeform Fabrication of Thin-Walled Structures," *J. Manuf. Sci. Eng.*, vol. 123, no. 4, pp. 615–622, 2001.
[10] T.-L. Teng, C.-P. Fung, and P.-H. Chang, "Effect of weld geometry and residual stresses on fatigue in butt-welded joints," *Int. J. Press. Vessels Pip.*, vol. 79, no. 7, pp. 467–482, Jul. 2002.
[11] L. Facchini, E. Magalini, P. Robotti, A. Molinari, S. Höges, and K. Wissenbach, "Ductility of a Ti-6Al-4V alloy produced by selective laser melting of prealloyed powders," *Rapid Prototyp. J.*, vol. 16, no. 6, pp. 450–459, Oct. 2010.
[12] A. H. Nickel, D. M. Barnett, and F. B. Prinz, "Thermal stresses and deposition patterns in layered manufacturing," *Mater. Sci. Eng. A*, vol. 317, no. 1, pp. 59–64, Oct. 2001.
[13] F. Calignano, "Design optimization of supports for overhanging structures in aluminum and titanium alloys by selective laser melting," *Mater. Des.*, vol. 64, pp. 203–213, Dec. 2014.
[14] B. Cheng and K. Chou, "Geometric consideration of support structures in part overhang fabrications by electron beam additive manufacturing," *Comput.-Aided Des.*, vol. 69, pp. 102–111, Dec. 2015.
[15] E. Coatanéa, R. Roca, H. Mokhtarian, F. Mokammel, and K. Ikkala, "A Conceptual Modeling and Simulation Framework for System Design," *Comput. Sci. Eng.*, vol. 18, no. 4, pp. 42–52, Jul. 2016.
[16] H. Mokhtarian *et al.*, "A Conceptual Design and Modeling Framework for Integrated Additive Manufacturing," *J. Mech. Des.*, vol. 140, no. 8, p. 081101, 2018.
[17] P. Bridgman, "Dimensional Analysis, 1922," *Phil Mag*, vol. 2, no. 12, pp. 1263–1266.
[18] N. Shadbolt and P. R. Smart, "Knowledge Elicitation: Methods, Tools and Techniques," in *Evaluation of Human Work*, J. R. Wilson and S. Sharples, Eds. CRC Press, 2015, pp. 163–200.
[19] T. L. Saaty, "The Modern Science of Multicriteria Decision Making and Its Practical Applications: The AHP/ANP Approach," *Oper. Res.*, vol. 61, no. 5, pp. 1101–1118, Oct. 2013.
[20] M. Yan and P. Yu, "An Overview of densification, microstructure and mechanical property of additively manufactured Ti-6Al-4V—Comparison among selective laser melting, electron beam melting, laser metal deposition and selective laser sintering, and with conventional powder," in *Sintering techniques of materials*, InTech, 2015.